Hindawi
Shock and Vibration
Volume 2019, Article ID 4351329, 11 pages
https://doi.org/10.1155/2019/4351329

Research Article

Analysis of the Effects of Soil on the Seismic Energy Responses of an Equipment-Structure System via Substructure Shaking Table Testing

Lanfang Luo,[1] **Nan Jiang**,[1,2] **and Jihong Bi**[1,2]

[1]*School of Civil Engineering, Tianjin University, Tianjin 300072, China*
[2]*Key Laboratory of Coastal Civil Engineering Structure and Safety, Tianjin University, Ministry of Education, Tianjin 300072, China*

Correspondence should be addressed to Nan Jiang; jiangnan@tju.edu.cn

Received 16 November 2018; Accepted 26 December 2018; Published 16 January 2019

Academic Editor: Stefano Sorace

This study investigated the real-time substructure shaking table testing (RTSSTT) of an equipment-structure-soil (ESS) system and the effects of soil on the seismic energy responses of the equipment-structure (ES) subsystem. First, the branch modal substructure approach was employed to derive the formulas needed for the RTSSTT of the ESS system. Then, individual equations for calculating the energy responses of the equipment and the structure were provided. The ES subsystem was adopted as the experimental substructure, whereas the reduced soil model was treated as the numerical substructure when the RTSSTT was performed on the ESS system. The effectiveness of the proposed testing method was demonstrated by comparing the test results with those of the integrated finite element analysis. The energy responses of the ES subsystem in the case of rigid ground (i.e., the ES system) were compared with those considering the effects of soil (i.e., the ESS system). The input energy responses of the ES subsystem were found to decrease significantly after taking the effects of soil into account. Differences due to the soil effects should be considered in the seismic design for the ES system.

1. Introduction

The seismic performance of the equipment-structure (ES) systems is gaining extensive attention of researchers because of the increasing use of the equipment and other nonstructural elements in modern buildings [1–4]. Most of the existing researches on ES interaction are based on the assumption that the ground is rigid, whereas a few studies have taken into consideration the effects of soil [5, 6]. The traditional shaking table testing method required the modeling of the whole ESS system, and the scale of testing was limited by the capacity of the shaking table used. Moreover, reproducing soil boundary conditions was technically complex. Real-time substructure testing [7] was proposed as a new method to study interactive shaking table model testing. In this method, the whole system was divided into experimental and numerical substructures. The experimental substructures were subjected to loads applied by the shaking table, the numerical substructures were simulated with numerical analysis software, and interactive data communication occurred between them. This method reduced the scale of testing while maintaining acceptable accuracy [8–10]. For the application of real-time substructure tests on an ESS system, a key point is the calculation of the interaction effects between the soil and the ES subsystem. Jiang and Yan [11] obtained the equation of motion for a soil-structure system using the branch modal substructure approach and analyzed the effects of soil in terms of a coupling load between the soil and the structure. However, the conventional branch modal substructure approach was applicable only to linear analysis as it involved modal reduction for all branches. Wang and Jiang [12] proposed an improved method called the mixed linear-nonlinear branch modal method, with which the effects of the nonlinear properties of the system could be included in the analysis.

Compared with acceleration, displacement, and other indicators of general seismic responses of the system, the energy component can give an improved reflection of seismic mechanisms and has the potential to address the effect of earthquake duration and cumulative damage of the system directly [13]. From the perspective of energy, the soil has the capacity for energy dissipation [14, 15], and energy transfer occurs between the soil and the upper structure during an earthquake [16, 17]. Thus, the response of the upper structure obtained in the research that considered the soil effects differs markedly from that obtained in the case of a rigid ground [18, 19]. Similarly, dynamic energy transfers between the equipment and the structure under seismic excitations, and this phenomenon is especially intense when frequency tuning takes place between the equipment and the structure. Studies have shown that the energy dissipation by the secondary structure (i.e., equipment) can alter the energy distribution in the primary structure [20, 21]. Taking the equipment, structure, and soil as a whole and analyzing the energy flow in the overall system can capture the seismic responses of the ES system more accurately and lead to a better understanding of the mechanism of interactions. However, these aspects have rarely been reported.

In the present study, the branch modal substructure approach was employed to derive the equation of motion for an ESS system. Energy response equations were derived for the ES subsystem, which allowed the energy responses of the equipment and the structure to be calculated separately in an analysis that included the soil effects. A scaled ESS model was treated as the research object. The ES subsystem was adopted as the experimental substructure, with the structure being a four-story steel frame structure and the equipment as a two-degree-of-freedom (2-DOF) model. The soil was treated as the numerical substructure. Ritz vectors were used to reduce its DOFs to ensure the implementation of RTSSTT. The shaking table test of the ES subsystem and the RTSSTT of the ESS system were performed, and the effects of soil on energy responses of the subsystem were examined through a comparative analysis of the testing results.

2. RTSSTT Method Based on the Branch Modal Substructure Approach

The equation of motion for an ESS system was derived based on the branch modal substructure approach. After transformation, the equation was applied to the real-time substructure testing of the system. Then, the equations for calculating the individual energy responses of the equipment and the structure were derived from the formulas involved in the RTSSTT of the system.

2.1. Equation of Motion for an ESS System. The ESS system comprised soil, structure, and equipment (Figure 1(a)). The system was divided into the following three branches using the branch modal substructure approach: branch d, rigid structure and rigid equipment on an elastic ground (Figure 1(b)); branch s, deformed structure and rigid equipment on a rigid ground (Figure 1(c)); and branch e, rigid structure and deformed equipment on a rigid ground (Figure 1(d)).

The characteristic equations for branch d are presented in equation (1), where k_d and m_d are the stiffness matrix and mass matrix, respectively, for the soil in branch d. Then, the modal transformation matrix composed of m-order modes was obtained:

$$\begin{aligned} [k_d]\{\phi_d\} &= \lambda_d [m_d]\{\phi_d\}, \\ [\Phi_d] &= \left[\{\phi\}_d^1 \cdots \{\phi\}_d^i \cdots \{\phi\}_d^m\right]. \end{aligned} \tag{1}$$

After modal transformation, the computational matrices for branch d can be expressed in the following forms:

$$\begin{aligned} \{u_d\} &= [\Phi_d]\{q_d\}, \\ \left[\widetilde{k}_d\right] &= [\Phi_d]^{\mathrm{T}}[k_d][\Phi_d], \\ [\widetilde{m}_d] &= [\Phi_d]^{\mathrm{T}}[m_d][\Phi_d], \\ [\widetilde{c}_d] &= [\Phi_d]^{\mathrm{T}}[c_d][\Phi_d], \\ \left[\widetilde{f}_d\right] &= [\Phi_d]^{\mathrm{T}}[f_d], \end{aligned} \tag{2}$$

where u_d and q_d represent the displacement coordinates and modal coordinates of the soil, respectively, in branch d. The damping matrix of the soil in branch d is represented by c_d, which can be obtained by the general damping theory. The load matrix of the branch d is represented by f_d. In practice, it is possible to reduce the computing scale for the soil by obtaining appropriate modes that meet accuracy requirements.

As the equipment and the structure had relatively small numbers of DOFs and their nonlinearity could not be neglected, complete computational matrices were created for them. The displacement u_s of the structure has two components: rigid-body displacement resulting from displacement of the soil (Figure 1(b)) and intrinsic displacement of the structure (Figure 1(c)), denoted by q_s. It was given by

$$\{u_s\} = [R_{sd}][\Phi_d]\{q_d\} + \{q_s\}. \tag{3}$$

R_{sd} can be determined from the rigid-body displacement of the structure resulting from the deformation of the soil in branch d.

The displacement u_e of the equipment can be broken down into three components: rigid-body displacement caused by the displacement of the soil (Figure 1(b)), rigid-body displacement caused by the displacement of the structure (Figure 1(c)), and intrinsic displacement of the equipment (Figure 1(d)), denoted by q_e:

$$\{u_e\} = [R_{ed}][\Phi_d]\{q_d\} + [R_{es}]\{q_s\} + \{q_e\}. \tag{4}$$

R_{ed} can be obtained from the rigid-body displacement of the equipment caused by the deformation of the soil in branch d. R_{es} can be obtained from the rigid-body displacement of the equipment caused by the structural deformation in branch s. The relationships among the displacements of the soil, structure, and equipment can be described in a matrix form as follows:

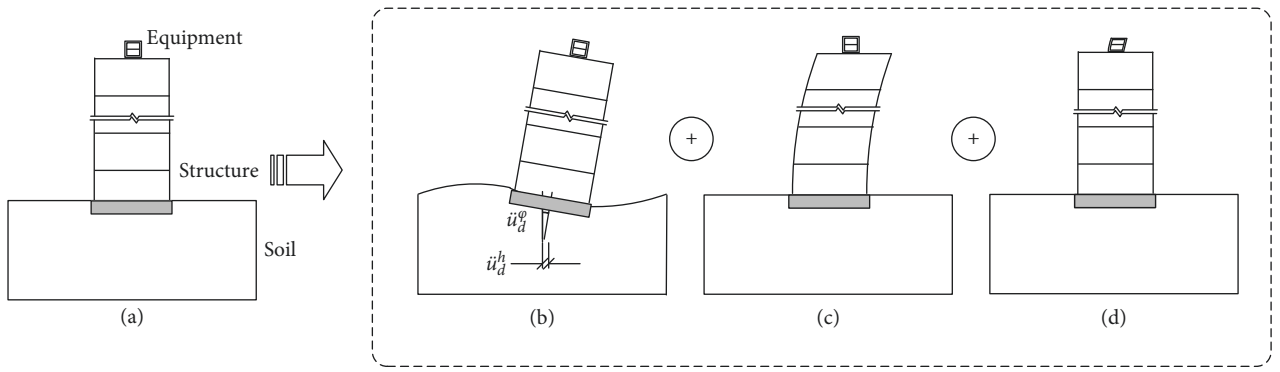

Figure 1: Schematic diagram of the equation of motion for the general ESS system. (a) ESS system. (b) Rigid structure and rigid equipment on an elastic soil. (c) Deformed structure and rigid equipment on a rigid soil. (d) Rigid structure and deformed equipment on a rigid soil.

$$\begin{Bmatrix} u_d \\ u_s \\ u_e \end{Bmatrix} = \begin{bmatrix} \Phi_d & 0 & 0 \\ R_{sd}\Phi_d & I & 0 \\ R_{ed}\Phi_d & R_{es} & I \end{bmatrix}. \tag{5}$$

Rearranging the equation based on the branch modal substructure approach yielded the following equation of motion for the ESS system:

$$\begin{bmatrix} \widetilde{m}_d & \Phi_d^{\mathrm{T}} R_{sd}^{\mathrm{T}} m_s & \Phi_d^{\mathrm{T}} R_{ed}^{\mathrm{T}} m_e \\ m_s R_{sd}\Phi_d & m_s & R_{es}^{\mathrm{T}} m_e \\ m_e R_{ed}\Phi_d & m_e R_{es} & m_e \end{bmatrix} \begin{Bmatrix} \ddot{q}_d \\ \ddot{q}_s \\ \ddot{q}_e \end{Bmatrix} + \begin{bmatrix} \widetilde{c}_d & 0 & 0 \\ 0 & c_s & 0 \\ 0 & 0 & c_e \end{bmatrix} \begin{Bmatrix} \dot{q}_d \\ \dot{q}_s \\ \dot{q}_e \end{Bmatrix} + \begin{bmatrix} \widetilde{k}_d & 0 & 0 \\ 0 & k_s & 0 \\ 0 & 0 & k_e \end{bmatrix} \begin{Bmatrix} q_d \\ q_s \\ q_e \end{Bmatrix} = \begin{Bmatrix} \widetilde{f}_d \\ f_s \\ f_e \end{Bmatrix}. \tag{6}$$

Moving the soil-structure coupling term $m_s R_{sd}\Phi_d$, the soil-equipment coupling term $m_e R_{ed}\Phi_d$, and the equipment-structure coupling term $m_e R_{es}$ to the right-hand side of equation (6) and rewriting in terms of load yielded the following individual equations of motion for the soil, structure, and equipment:

$$\widetilde{m}_d\ddot{q}_d + \widetilde{c}_d\dot{q}_d + \widetilde{k}_d q_d = \widetilde{f}_d - \Phi_d^{\mathrm{T}} R_{sd}^{\mathrm{T}} m_s \ddot{q}_s - \Phi_d^{\mathrm{T}} R_{ed}^{\mathrm{T}} m_e \ddot{q}_e, \tag{7}$$

$$m_s\ddot{q}_s + c_s\dot{q}_s + k_s q_s = f_s - m_s R_{sd}\Phi_d\ddot{q}_d - R_{es}^{\mathrm{T}} m_e \ddot{q}_e, \tag{8}$$

$$m_e\ddot{q}_e + c_e\dot{q}_e + k_e q_e = f_e - m_e R_{ed}\Phi_d\ddot{q}_d - m_e R_{es}\ddot{q}_s, \tag{9}$$

where m_s, c_s, and k_s represent, respectively, the mass matrix, damping matrix, and stiffness matrix of the structure in branch s; m_e, c_e, and k_e denote the mass matrix, damping matrix, and stiffness matrix, respectively, of the equipment in branch e; f_s and f_e are the load matrices for the structure and the equipment, respectively; q_s is the displacement of the structure relative to the ground; and q_e is the displacement of the equipment relative to the top floor of the structure.

The right-hand sides of the equations of motion for the soil, structure, and equipment all contain coupling loads arising from their interactions (see equations (7)–(9)). The data exchange between the substructures is realized by the transmission of the coupling term loads. The total load acting on the ES subsystem is illustrated in Figure 2.

In Figure 2, $\ddot{u}_d^h$ is the translational acceleration of the foundation and $\ddot{u}_d^\varphi$ is its rotational acceleration. The effect of $\ddot{u}_d^\varphi$ depended on the height of each DOF of the ES subsystem. $\ddot{u}_d^\varphi$ was converted to an equivalent horizontal load to achieve the rotation effect of the foundation on the horizontal shaking table test:

$$m_s^1\left(\ddot{u}_g + \ddot{u}_d^h + \ddot{u}_d^\varphi h_1\right) + m_s^2\left(\ddot{u}_g + \ddot{u}_d^h + \ddot{u}_d^\varphi h_2\right) + \ldots + m_e^n\left(\ddot{u}_g + \ddot{u}_d^h + \ddot{u}_d^\varphi h_n\right) = m_s^1\ddot{u}_{\mathrm{eq}} + m_s^2\ddot{u}_{\mathrm{eq}} + \ldots + m_e^n\ddot{u}_{\mathrm{eq}}. \tag{10}$$

Then, the equivalent translational acceleration $\ddot{u}_{\mathrm{eq}}$ applied by the shaking table in a uniform manner can be expressed as follows:

$$\ddot{u}_{\mathrm{eq}} = \ddot{u}_g + \ddot{u}_d^h + \frac{m_s^1 h_1 + m_s^2 h_1 + \ldots + m_e^n h_n}{m_s^1 + m_s^2 + \ldots + m_e^n}\ddot{u}_d^\varphi. \tag{11}$$

This study treated soil as the numerical substructure and the ES subsystem as the experimental substructure. The interaction between the soil and the structure was achieved by the data exchange of the coupling loads in equations (7)–(9). The soil was subjected to the load of the structure and the equipment equation (7). The effects of soil on the structure was transmitted by the coupling term load in equation (8), whereas the interaction between the structure and the equipment, considering the effect of the soil in equation (9), relied on their physical connection. The substructure testing procedure for an ESS system included the following specific steps:

(1) First, the total load on the soil (as shown on the right-hand side of its equation of motion) was assumed to

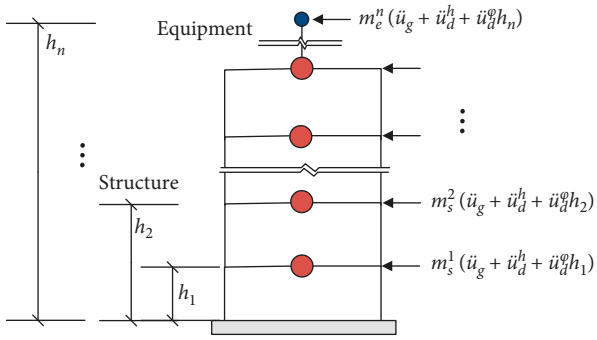

Figure 2: Load on the ES subsystem.

be known, and the acceleration response of the soil was computed

(2) The coupling term load between the soil and the structure was calculated using equation (8) and applied to the ES subsystem via the shaking table

(3) Based on the acceleration responses collected from the ES subsystem, the overall load experienced by the soil at the next moment can be calculated using equation (7), and the corresponding acceleration response of the soil can be calculated again

The aforementioned steps were repeated until the testing ended, and the responses of different components of the ESS system were obtained.

2.2. Energy Response Equations. The energy responses of the structure and the equipment were calculated based on their own equations of motion. Integrating both sides of the equations with respect to their displacements dq_s and dq_e, respectively, over the time interval $[0, t_0]$ yielded their energy response equations as follows:

$$\int_0^{t_0} \dot{q}_s^{\mathrm{T}} m_s \ddot{q}_s d(t) + \int_0^{t_0} \dot{q}_s^{\mathrm{T}} c_s \dot{q}_s d(t) + \int_0^{t_0} \dot{q}_s^{\mathrm{T}} k_s q_s d(t) = \int_0^{t_0} \dot{q}_s^{\mathrm{T}} \left(f_s - m_s R_{sd} \Phi_d \ddot{q}_d - R_{es}^T m_e \ddot{q}_e \right) d(t), \tag{12}$$

$$\int_0^{t_0} \dot{q}_e^{\mathrm{T}} m_e \ddot{q}_e d(t) + \int_0^{t_0} \dot{q}_e^{\mathrm{T}} c_e \dot{q}_e d(t) + \int_0^{t_0} \dot{q}_e^{\mathrm{T}} k_e q_e d(t) = \int_0^{t_0} \dot{q}_e^{\mathrm{T}} \left(f_e - m_e R_{ed} \Phi_d \ddot{q}_d - m_e R_{es} \ddot{q}_s \right) d(t). \tag{13}$$

The terms on the right-hand sides of equations (12) and (13) represent the energy input to the structure, E_{IS}, and to the equipment, E_{IE}, respectively.

3. Application of RTSSTT

The RTSSTT of an ESS system was performed on the shaking table with dimensions of $3 \times 3\,\mathrm{m}^2$ at Beijing University of Technology. Uniaxial loading was adopted. El Centro, TianJin, and PerSon ground motions, which were suitable for type III site, were used as the seismic inputs, where El Centro and TianJin ground motions were earthquake records and PerSon ground motion was an artificial seismic motion. The time history of the corresponding ground acceleration is presented in Figure 3. The timescale factors for the three ground motions were 0.45. For the requirements of level VIII seismic intensity, the acceleration amplitudes of the three ground motions were adjusted to $0.7\,\mathrm{m/s}^2$ during a minor earthquake and to $2.0\,\mathrm{m/s}^2$ during a moderate earthquake. As equipment may collapse and the structure may be greatly damaged during major earthquakes, considering that the structure will be used in the following related researches, this study did not consider major earthquake conditions.

3.1. Experimental Substructure Model. A one-fifth scale model of an ES subsystem used in the RTSSTT tests is shown in Figure 4. The four-floor steel frame structure model was constructed with H-beams with a cross section of dimension $100 \times 45 \times 6 \times 8\,\mathrm{mm}^4$. The floor height was 0.63 m, except for the first floor with a height of 0.68 m. The longitudinal and transverse spans of the structure were both 1.6 m. Each of the lower three floors had a total mass of 1700 kg, whereas the fourth floor weighed 1540 kg. The structural material had an elastic modulus of 202.0 GPa and a yield strength of 339.6 MPa. The 2-DOF model of communication equipment was made of a round steel pipe. Each layer of the equipment measured 0.25 m high and weighed 90 kg. The equipment material had an elastic modulus of 192.0 GPa and a yield strength of 421.4 MPa.

3.2. Numerical Substructure Model. The material parameters of the foundation and soil are provided in Table 1. Artificial boundaries were introduced to simulate the effects of radiation damping of the unbounded soil media. The finite element model of soil, constructed using ANSYS, had an overall dimension of $30 \times 15 \times 15\,\mathrm{m}^3$, and a foundation with a dimension of $2.2 \times 2.2 \times 0.4\,\mathrm{m}^3$ was embedded into it. The height ($h_{\max}$) and the width ($b_{\max}$) of the soil elements satisfied the following conditions: $h_{\max} = (0.200 - 0.125)\lambda_s$ (where λ_s is the wavelength) and $b_{\max} \le 0.5\ h_{\max}$. The soil model was designed with a fixed bottom and viscoelastic lateral boundaries (Figure 5). Rayleigh damping was used for it, with a damping ratio of 0.2. Subsequently, the computational matrices for the soil model were derived. According to the Ritz vector method provided in a previous study [22], the modes and frequencies of the soil were calculated and the first 60 modes and frequencies were truncated to obtain a total mass participation factor of 0.95. Then, the modal transformation matrix Φ_d for the soil model was obtained. Furthermore, the computational matrices for the soil model after reduction were derived. In this way, the amount of computation was reduced in the precondition of precision ensuring. The modal reduced soil model can satisfy the real-time requirement.

3.3. Testing System and Control Method. This study provides a brief description of the real-time substructure testing system. The complete real-time substructure experimental system consisted of a specialized engineering computer, a compiler, and input/output (I/O) devices. SIMULINK was installed on

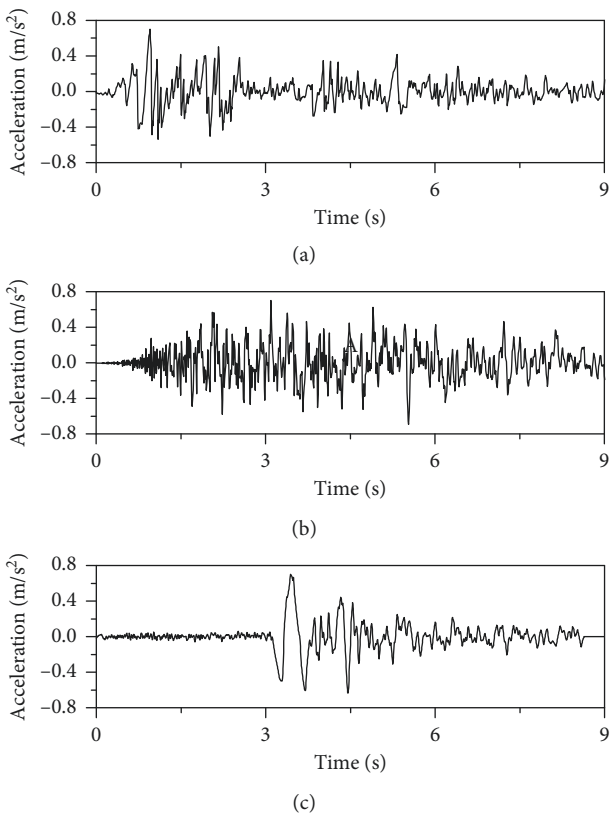

Figure 3: Acceleration time-history curves of the three ground motions. (a) El Centro. (b) PerSon. (c) TianJin.

the computer for computing the numerical substructure and designing controllers. The I/O devices served to input the data acquired from the experimental substructure and output the computational data from the numerical substructure. The description of the loading device used in real-time substructure testing has a great influence on the accuracy of testing. In order to track accurately the performance of the shaking table, an approach that combined real-time numerical feedback control and physical feedback control was used for the controller design (see Figure 6(a)). The inverse dynamic compensation strategy, as reported elsewhere [23, 24], was used for modeling certain dynamics of the shaking table in a real-time numerical feedback control loop.

The transfer function which was used in the numerical feedback control loop was identified using MATLAB based on the reference signal and the measured acceleration of the shaking table:

$$G = \frac{2.611 \times 10^8}{s^4 + 913.6s^3 + 9.525 \times 10^4 s^2 + 1.245 \times 10^7 s + 2.613 \times 10^8}. \quad (14)$$

Figure 6(b) shows the comparative results of amplitudes and phases from the shaking table testing and the systematic identification. As can be observed, the results in these two cases coincide in terms of their overall trends, demonstrating that the transfer function fitted by the systematic identification is capable of describing the actual vibrational motion of the shaking table. Then, the physical part is driven by the shaking table controller, which helps to provide more accurate tracking and control of the shaking table trajectory.

3.4. Computational Module for Testing. During testing, computational module and real-time energy output module were developed for the numerical substructure and experimental substructure, respectively. The computational module for the numerical substructure is shown in Figure 7.

In Figure 7, $\ddot{u}_g$ represents earthquake excitation, f_{sd} represents the coupling load between soil and structure, f_{ed} is the coupling load between soil and equipment, and x is a state variable composed of the modal displacement and modal velocity of the soil. The input variable u comprises the external and coupling loads. The output variable y denotes the physical acceleration of the soil after a coordinate transformation. $\ddot{u}_{out}$ denotes the translational and rotational accelerations of the soil. The equivalent translational acceleration obtained using (11) was used as the actual seismic excitation to which the experimental substructure was subjected. A, B, C, and D in the equations can be expressed as follows:

$$[A] = \begin{bmatrix} 0 & I \\ -\dfrac{\tilde{k}_d}{\tilde{m}_d} & -\dfrac{\tilde{c}_d}{\tilde{m}_d} \end{bmatrix},$$

$$[B] = \begin{bmatrix} 0 & 0 & 0 \\ \dfrac{1}{\tilde{m}_d} & \dfrac{1}{\tilde{m}_d} & \dfrac{1}{\tilde{m}_d} \end{bmatrix}, \quad (15)$$

$$[C] = \begin{bmatrix} -\dfrac{\Phi_d \tilde{k}_d}{\tilde{m}_d} & -\dfrac{\Phi_d \tilde{c}_d}{\tilde{m}_d} \end{bmatrix},$$

$$[D] = \begin{bmatrix} \dfrac{\Phi_d}{\tilde{m}_d} & \dfrac{\Phi_d}{\tilde{m}_d} & \dfrac{\Phi_d}{\tilde{m}_d} \end{bmatrix}.$$

In the energy response computation, Rayleigh damping was used for the structure and the equipment. The equipment was represented by a 2-DOF model. Each layer of the equipment had a stiffness of 744,368 N/m and damping of 174.5 N/(m/s). The structure was numerically simulated by a 4-DOF shear model obtained from the aforementioned parameters. Each of the lower three floors had a mass of 1700 kg, whereas the fourth floor weighed 1540 kg. The first floor had a stiffness of 2,423,080 N/m and damping of 4463 N/(m/s), whereas each of the upper three floors had a stiffness of 3,833,120 N/m and damping of 7061 N/(m/s). Acceleration responses of different parts of the structure and the equipment were measured using 941B sensors during testing. After being processed by filtering, the collected data were used to derive the corresponding velocity and displacement responses through integration.

Considering, for example, the real-time energy output module for the structure, Figure 8 shows the schematic representation of the output module for the input energy of the structure. In this figure, vel denotes the relative velocity

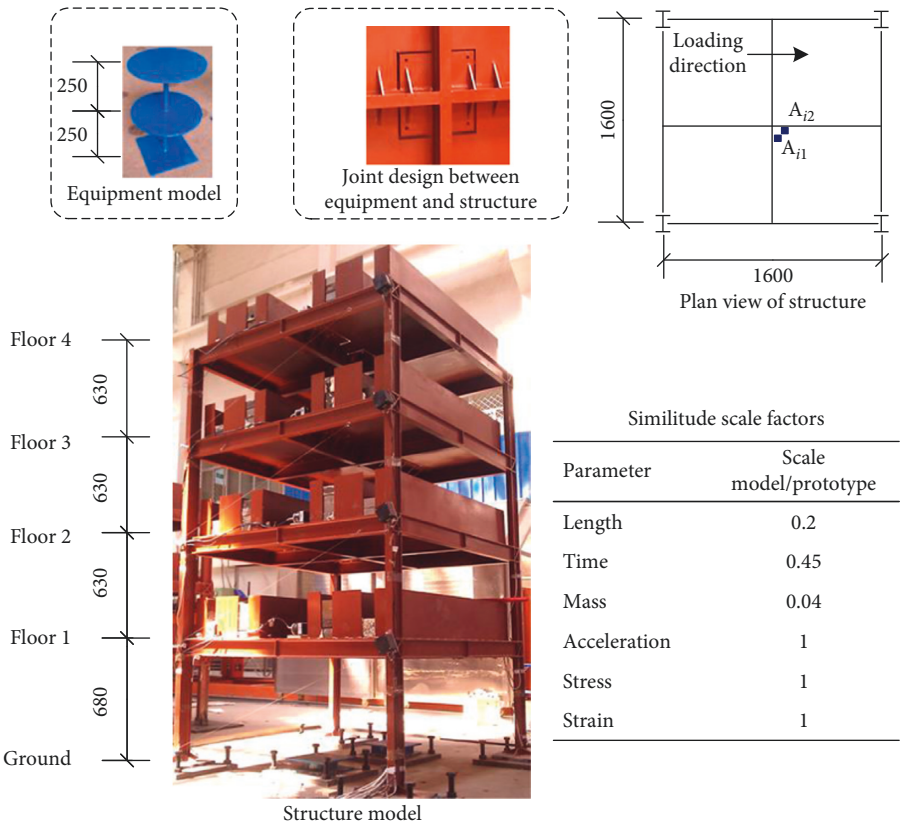

Similitude scale factors

Parameter	Scale model/prototype
Length	0.2
Time	0.45
Mass	0.04
Acceleration	1
Stress	1
Strain	1

Figure 4: Design model of the ES subsystem.

Table 1: Material parameters of the foundation and soil.

Type	Depth (m)	Elastic modulus (Pa)	Density (kg/m^3)	Viscous force (Pa)	Friction angle (°)
Foundation	0.4	3.52×10^{10}	2650	—	—
Soil layer 1	3.6	2.11×10^{7}	1730	1.25×10^{4}	15.3
Soil layer 2	8.4	5.64×10^{7}	1950	1.65×10^{4}	16.8
Soil layer 3	3.0	3.37×10^{8}	2030	1.84×10^{4}	21.6

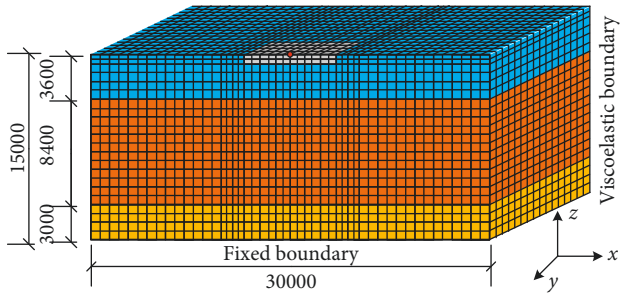

Figure 5: Design model of the numerical substructure.

response of the structure, f_{es} denotes the coupling load between the equipment and the structure, and Earth represents the seismic excitation of the structure, which is earthquake records in the case of rigid ground and absolute acceleration when considering the effects of soil. The input energy responses of the structure can be obtained using (12) via the matrix multiply and discrete-time integrator modules in SIMULINK. As the real-time energy output module for the equipment is similar to this one, it is not described in this study.

4. Results and Analysis

The reliability of the real-time substructure testing method proposed was validated by comparing the testing results of the ESS system with the results of the integrated finite element analysis. Then, the effects of soil on the energy responses of the ES subsystem were analyzed from the perspective of input energy.

4.1. Validation of the Testing Method. An integrated finite element analysis was performed using Matlab. The computational matrices for soil presented earlier were used in this analysis. The structure and equipment were modeled with the aforementioned multiple DOF models. Then, the results of the integrated finite element analysis and the

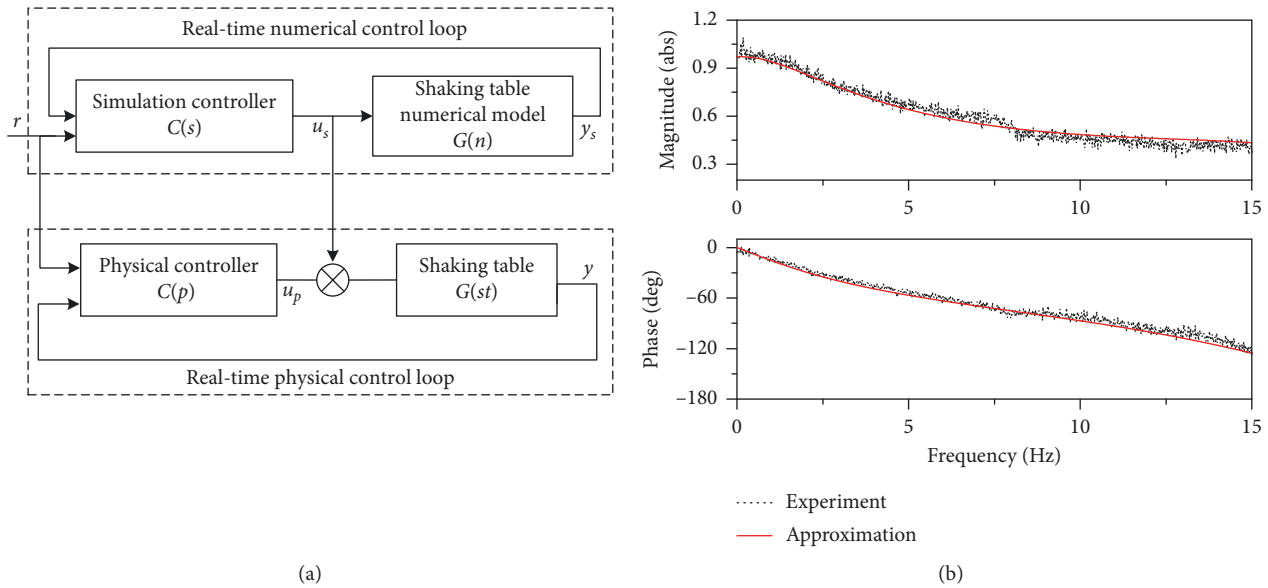

Figure 6: Principle and accuracy of the control method. (a) Principle of control method. (b) Comparison of the experimental and approximated transfer functions of the shaking table.

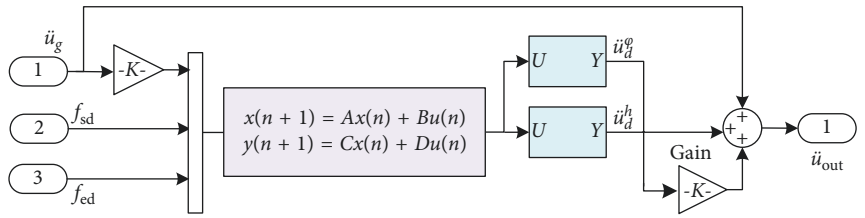

Figure 7: Computational module for the numerical substructure.

substructure testing were compared in terms of an acceleration response of the equipment top relative to the structure top at an input peak ground acceleration (PGA) of 0.7 m/s^2 (Figure 9).

As shown in Figure 9, the acceleration responses of the equipment top obtained by the two methods were roughly consistent. The peak accelerations of equipment under El Centro, PerSon, and TianJin ground motions in the RTSSTT decreased by 5.7%, 8.9%, and 7.3%, respectively, than those obtained in the integrated finite element analysis. In the real-time substructure testing, errors were attributable mainly to differences between the numerical and experimental models of the ES subsystem and the accuracy of the control method used in the testing. Overall, the real-time substructure testing method based on the branch modal substructure approach was reliable, valid, and able to deliver the desired accuracy.

4.2. Effect of Soil on the Energy Response of the ES System. Shaking table tests were performed on the ES subsystem (case I: rigid ground) and ESS system (case II: considering the effects of soil). In the tests of case I, earthquake ground motions were directly applied to the ES subsystem. The input energy responses of the ES subsystem by the end of ground motion under different conditions are displayed in Tables 2 and 3. In the tables, Acc represents the PGA of the original seismic input of the shaking table, and the symbols EL, PS, and TJ denote El Centro, PerSon, and TianJin ground motions, respectively. Figures 10 and 11 show the time-history curves of the equipment's input energy under different ground motions.

As shown in Figures 10 and 11, the input energy curves of the equipment followed an overall downward trend compared with those in case I, and the rate of decrease differed between different ground motions. For example, at an input PGA of 0.7 m/s^2, the input energy of the equipment decreased by 54.26% and 64.82%, respectively, by the end of El Centro and TianJin ground motions, higher than the 24.58% decline under PerSon ground motion, than those observed in case I. A comparison between the results under different input amplitudes revealed that the effect of the soil on the energy responses of the equipment related to the intensity of the seismic inputs. The input energy of the equipment under El Centro, PerSon, and TianJin ground motions at an input PGA of 2.0 m/s^2 decreased by 33.87%, 8.96%, and 47.52%, respectively, than those observed in case I, which was lower than that at an input PGA of 0.7 m/s^2. Moreover, a comparison of the time-history curves of input energy in cases I and II revealed a smoother and steadier time history in case II.

These phenomena suggested that the effects of the soil reduced the input energy of the equipment and made its

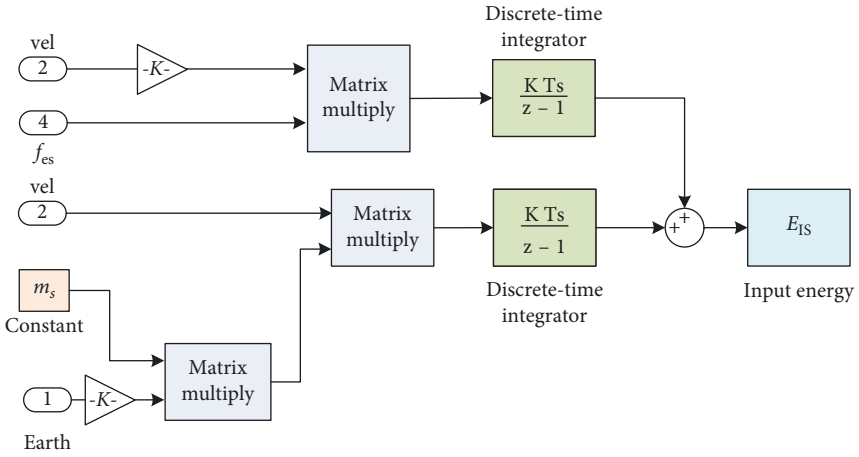

Figure 8: Real-time energy output module for the input energy of the structure.

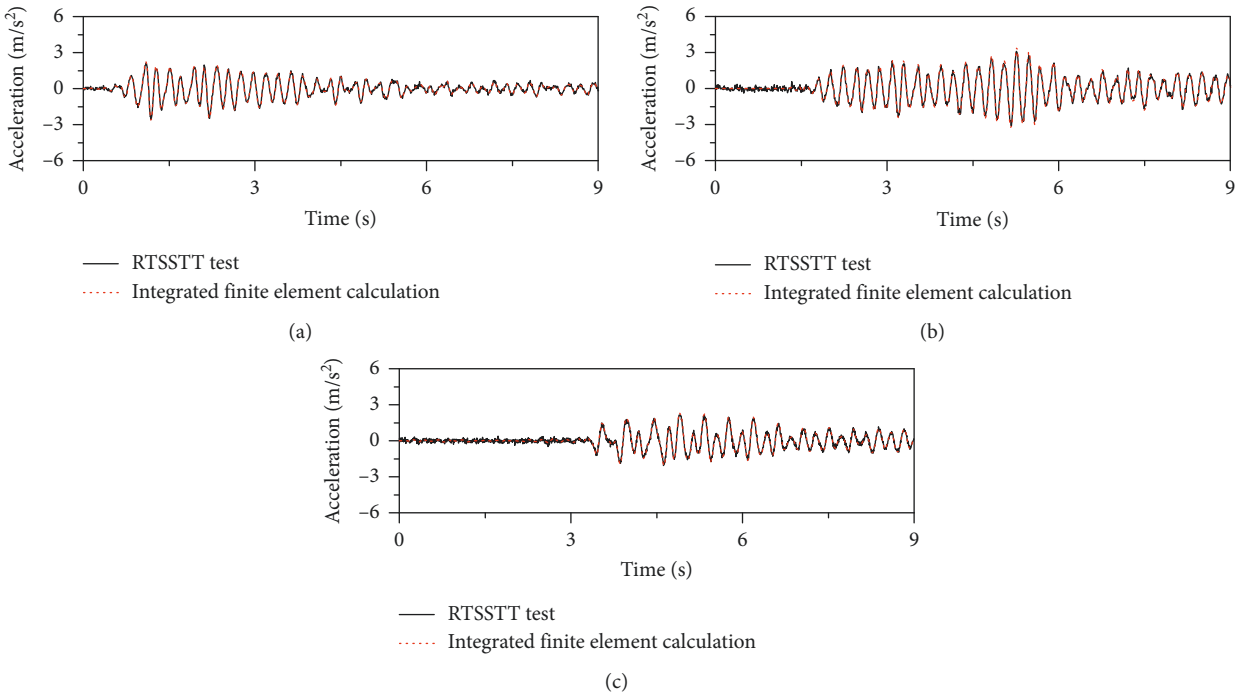

Figure 9: Comparison of acceleration responses of the equipment top. (a) El Centro. (b) PerSon. (c) TianJin.

Table 2: Energy responses of the ES subsystem in case I.

Types	Acceleration (m/s^2)	E_{IE} (J)	E_{IS} (J)
EL	0.7	0.6362	39.4420
	2.0	3.9234	307.9460
PS	0.7	0.9360	7.6200
	2.0	6.8576	87.7428
TJ	0.7	1.1047	107.5330
	2.0	6.3685	914.2232

Table 3: Energy responses of the ES subsystem in case II.

Types	Acceleration (m/s^2)	E_{IE} (J)	E_{IS} (J)
EL	0.7	0.2910	7.8793
	2.0	2.5944	138.7004
PS	0.7	0.7059	3.8884
	2.0	6.2432	70.8925
TJ	0.7	0.3886	31.2895
	2.0	3.3420	454.2743

energy responses more likely to decay than in the case of the rigid ground. In addition to the characteristics of the ground motion, the effects of the soil on the energy responses of the equipment also depended on the intensity of the seismic inputs: it tends to be weakened as the seismic intensity increases.

Figures 12 and 13 show the time-history curves of the input energy of the structure under different ground motions.

The energy responses of the structure demonstrated that the soil had a similar effect on the energy responses of the

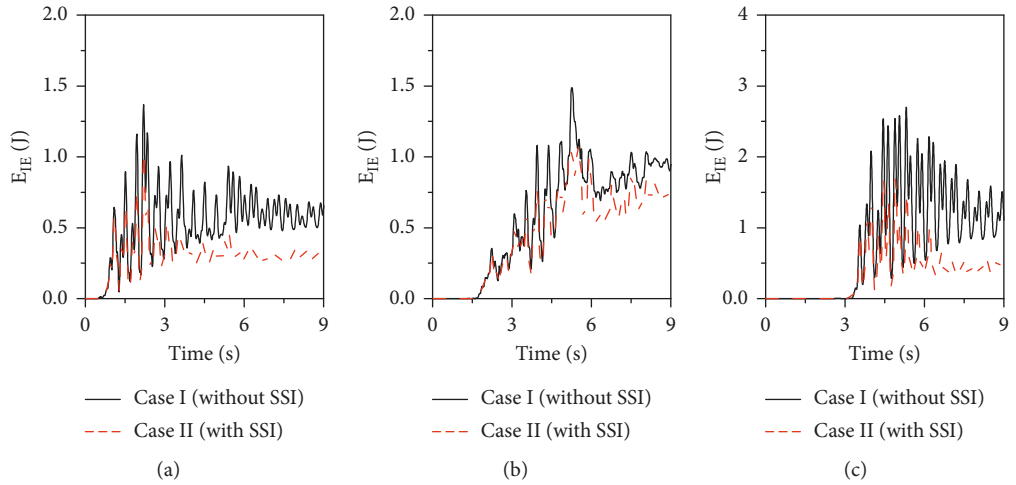

Figure 10: Time-history curves of the input energy of the equipment at an input PGA of 0.7 m/s^2. (a) El Centro. (b) PerSon. (c) TianJin.

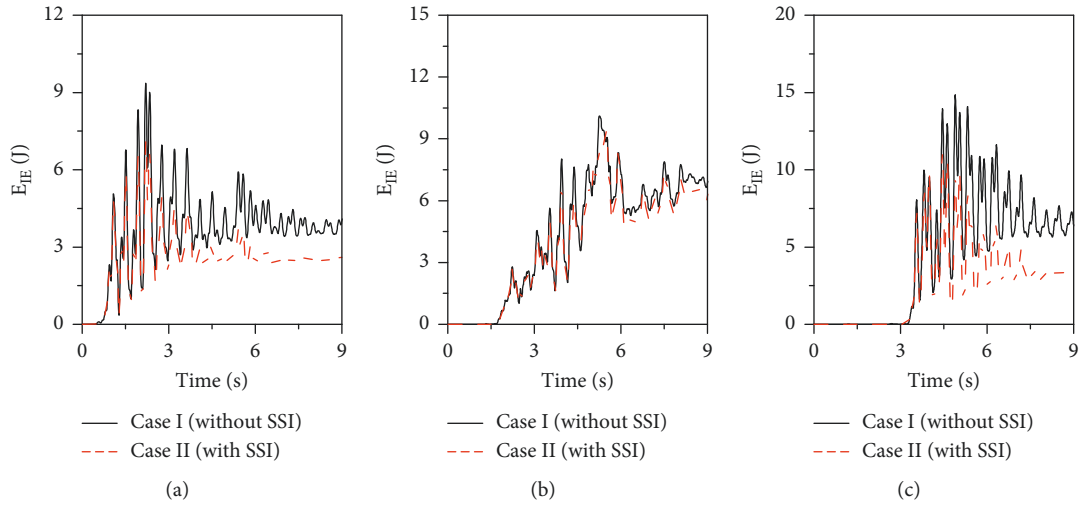

Figure 11: Time-history curves of the input energy of the equipment at an input PGA of 2.0 m/s^2. (a) El Centro. (b) PerSon. (c) TianJin.

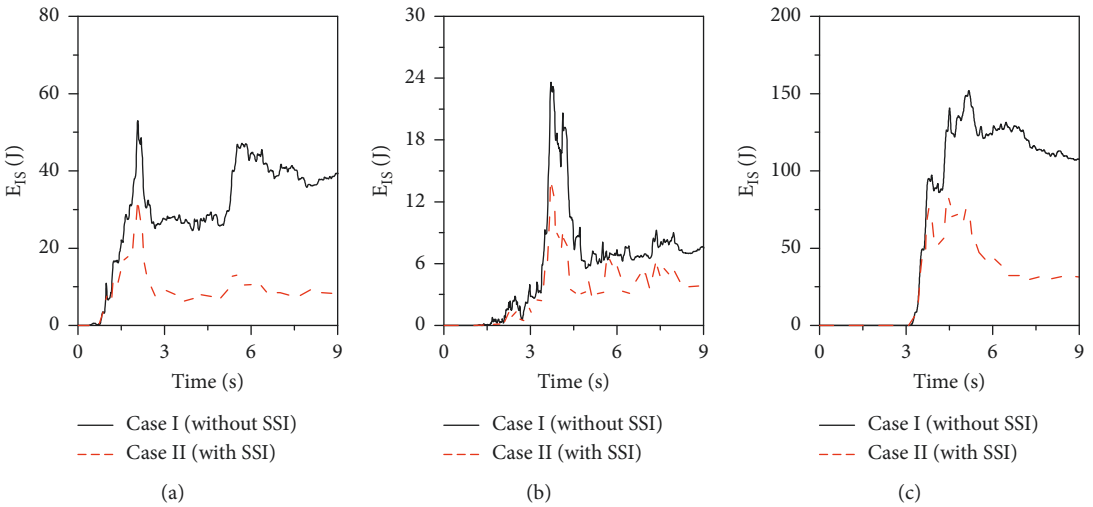

Figure 12: Time-history curves of the input energy of the structure at an input PGA of 0.7 m/s^2. (a) El Centro. (b) PerSon. (c) TianJin.

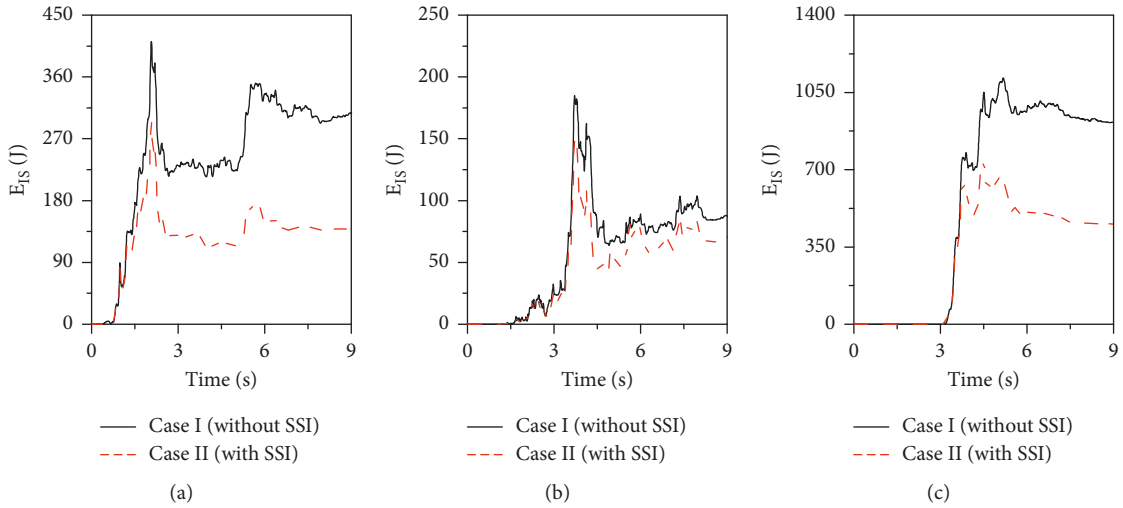

Figure 13: Time-history curves of the input energy of the structure at an input PGA of 2.0 m/s^2. (a) El Centro. (b) PerSon. (c) TianJin.

structure as that on the equipment. After considering the effects of the soil, the input energy responses of the structure decreased and the corresponding time-history curves became smoother. The decrease in the input energy of the structure was most significant under El Centro and TianJin ground motions at an input PGA of 0.7 m/s^2. The corresponding decreases by the end of the ground motions were 80.02% and 70.90%. As the input amplitude increased, the effect of the soil on the energy responses of the structure became weaker. At an input PGA of 2.0 m/s^2, the input energy of the structure under the two ground motions decreased by 54.96% and 50.31%, respectively, compared with those in the case of the rigid ground. These results indicated that the soil can attenuate the energy responses of the structure, and the magnitude of its effect varied with the intensity of the seismic inputs: an increase in the seismic intensity was associated with a decline in the effect of the soil on the energy responses of the structure.

In conclusion, it is considered that the influence of the soil will cause changes in the input energy to the equipment and structure. After considering the effects of soil, the total energy input and its distribution characteristics can be changed significantly. Additionally, the magnitude of the effects of the soil on the responses of the equipment and the structure depended on the intensity of the seismic inputs. As the intensity of the seismic inputs increased, the effects of the soil became weaker. Special attention should be paid to such effects in the design of the ES system.

5. Conclusions

In this study, the branch modal substructure approach was employed to derive the equations needed for the RTSSTT of an ESS system, and the individual equations for calculating the energy responses of the equipment and the structure were provided. The shaking table model testing of the ES system and the RTSSTT of the ESS system were performed. The real-time output of seismic energy responses of the experimental substructure was achieved using the equations combined with real-time substructure testing. The effects of soil on the energy responses of the ES system were investigated. The main conclusions are as follows:

(1) The branch modal substructure approach can be used to derive the equations of motion for the ESS system, which can remove the redundant DOF of the soil in the precondition of high-computational efficiency and precision ensuring. The modal reduced soil model can be directly allowed to implement real-time substructure testing.

(2) A comparative analysis revealed small differences and similar trends between the results of the RTSSTT and the integrated finite element analysis, demonstrating the validity and reliability of the RTSSTT method based on the branch modal substructure approach.

(3) An energy calculation method for the energy responses of each part in the ES subsystem has been proposed. Combined with the RTDSST tests, a method of real-time energy calculation also has been proposed to evaluate the energy variations of the structure and equipment during the process of testing, thus facilitating a study of the effects of soil on the energy responses of the equipment and structure.

(4) After considering the effects of soil, the input energy in the equipment and the structure decreased significantly. Designs of the equipment and the structure, based on an assumption of rigid ground, may be conservative.

Data Availability

The data in figures used to support the findings of this study are available from the corresponding author upon request.

Conflicts of Interest

The authors declare that there are no conflicts of interest regarding the publication of this paper.

Acknowledgments

This work was financially supported by the National Science Foundation Project (Research Project no. 51478312), China.

References

[1] J. Li, H. Chen, and Z. Sun, "Shaking table tests on spatial structure-equipment model systems," *Engineering Mechanics*, vol. 20, no. 1, pp. 157–161, 2003.

[2] M. Ismail, J. Rodellar, and F. Ikhouane, "Performance of structure-equipment systems with a novel roll-n-cage isolation bearing," *Computers & Structures*, vol. 87, no. 23-24, pp. 1631–1646, 2009.

[3] A. Filiatrault and T. Sullivan, "Performance-based seismic design of nonstructural building components: the next frontier of earthquake engineering," *Earthquake Engineering and Engineering Vibration*, vol. 13, no. 1, pp. 17–46, 2014.

[4] M. C. Chen, E. Pantoli, X. Wang et al., "Full-Scale structural and nonstructural building system performance during earthquakes: Part I–specimen description, test protocol and structural response," *Earthquake Spectra*, vol. 32, no. 2, pp. 737–770, 2015.

[5] S. R. Chaudhuri and V. K. Gupta, "Mode acceleration approach for generation of floor spectra including soil-structure interaction," *Journal of Earthquake Technology*, vol. 40, no. 213, pp. 99–115, 2003.

[6] E. Lim, X. Qin, and N. Chouw, "Dynamic interaction of a primary-secondary system considering soil- structure interaction," in *Proceedings of 6th International Confererence on Earthquake Geotechnical Engineering*, Christchurch, New Zealand, November 2015.

[7] M. Nakashima, H. Kato, and E. Takaoka, "Development of real-time pseudo dynamic testing," *Earthquake Engineering & Structural Dynamics*, vol. 21, no. 1, pp. 79–92, 1992.

[8] S.-K. Lee, E. C. Park, K.-W. Min, S.-H. Lee, L. Chung, and J.-H. Park, "Real-time hybrid shaking table testing method for the performance evaluation of a tuned liquid damper controlling seismic response of building structures," *Journal of Sound and Vibration*, vol. 302, no. 3, pp. 596–612, 2007.

[9] S. Günay, K. Mosalam, and S. Takhirov, "Real-time hybrid simulation in a shaking table configuration for parametric studies of high-voltage equipment and IEEE693 development," *Nuclear Engineering and Design*, vol. 295, pp. 901–909, 2015.

[10] K. M. Mosalam, S. Günay, and S. Takhirov, "Response evaluation of interconnected electrical substation equipment using real-time hybrid simulation on multiple shaking tables," *Earthquake Engineering & Structural Dynamics*, vol. 45, no. 14, pp. 2389–2404, 2016.

[11] X. L. Jiang and S. C. Yan, "Two step method of the branched modal and its use for liquid-structure-pile-soil interaction system," *Journal of Vibration Engineering*, vol. 7, no. 4, pp. 346–350, 1994.

[12] F. Wang and X. L. Jiang, "Analysis of soil structure interaction system based on mixed branch mode and constrained mode two-step method," *Journal of Earthquake Engineering and Engineering Vibration*, vol. 30, no. 4, pp. 24–30, 2010.

[13] E. Bojórquez, A. Terán-Gilmore, S. E. Ruiz, and A. Reyes-Salazar, "Evaluation of structural reliability of steel frames: interstory drift versus plastic hysteretic energy," *Earthquake Spectra*, vol. 27, no. 3, pp. 661–682, 2011.

[14] S. Gajan and D. S. Saravanathiiban, "Modeling of energy dissipation in structural devices and foundation soil during seismic loading," *Soil Dynamics and Earthquake Engineering*, vol. 31, no. 8, pp. 1106–1122, 2011.

[15] V. Gičev and M. D. Trifunac, "Energy dissipation by nonlinear soil strains during soil–structure interaction excited by SH pulse," *Soil Dynamics and Earthquake Engineering*, vol. 43, no. 4, pp. 261–270, 2012.

[16] I. Takewaki, "Bound of earthquake input energy to soil-structure interaction systems," *Soil Dynamics and Earthquake Engineering*, vol. 25, no. 7–10, pp. 741–752, 2005.

[17] K. Kojima, K. Sakaguchi, and I. Takewaki, "Mechanism and bounding of earthquake energy input to building structure on surface ground subjected to engineering bedrock motion," *Soil Dynamics and Earthquake Engineering*, vol. 70, pp. 93–103, 2015.

[18] M. D. Trifunac, "Nonlinear soil response as a natural passive isolation mechanism. Paper II. The 1933, long beach, California earthquake," *Soil Dynamics and Earthquake Engineering*, vol. 23, no. 7, pp. 549–562, 2003.

[19] H. Y. Zhuang, X. Yu, C. Zhu, and D. D. Jin, "Shaking table tests for the seismic response of a base-isolated structure with the SSI effect," *Soil Dynamics and Earthquake Engineering*, vol. 67, no. 6, pp. 208–218, 2014.

[20] K. K. Wong, "Seismic energy dissipation of inelastic structures with tuned mass dampers," *Journal of Engineering Mechanics*, vol. 134, no. 2, pp. 163–172, 2008.

[21] P. Tan, X. X. Li, L. K. Liu, and Y. Zhang, "Control mechanism and performance analysis of a mega-sub structure control system," *China Civil Engineering Journal*, vol. 47, no. 11, pp. 55–63, 2014.

[22] Y. Li and X. Jiang, "Parametric analysis of eccentric structure-soil interaction system based on branch mode decoupling method," *Soil Dynamics and Earthquake Engineering*, vol. 48, no. 6, pp. 63–70, 2013.

[23] Y. Tagawa, J. Y. Tu, and D. P. Stoten, "Inverse dynamics compensation via "simulation of feedback control systems"," *Proceedings of the Institution of Mechanical Engineers Part I Journal of Systems and Control Engineering*, vol. 225, no. 1, pp. 137–153, 2010.

[24] Z. Y. Tang, S. C. Chen, J. X. Zhang, and Z. B. Li, "Study on the stability prediction of real-time dynamic substructuring system based on shaking table," *Engineering Mechanics*, vol. 33, no. 12, pp. 217–224, 2016.